Hindawi
Advances in Meteorology
Volume 2024, Article ID 6819711, 14 pages
https://doi.org/10.1155/2024/6819711

Research Article

False Alarm Causes and Wind Field Sensitivity Analysis of a Severe Rainfall Event in the Guangdong-Hong Kong-Macao Greater Bay Area Urban Cluster

Lan Zhang,[1] Jiawen Zheng,[1] Huaiyu Li,[1] Rui Yu,[2] Lei Wei,[1] and Yufei Zhang[3]

[1]*Guangzhou Meteorological Observatory, Guangzhou 511430, China*
[2]*Nanhai Meteorological Service, Foshan 528200, China*
[3]*Guangzhou Meteorological Public Service Center, Guangzhou 511400, China*

Correspondence should be addressed to Jiawen Zheng; karmanzheng@163.com

Received 1 November 2023; Revised 21 January 2024; Accepted 13 February 2024; Published 4 March 2024

Academic Editor: Hiroyuki Hashiguchi

On May 11, 2022, despite the favorable upper and lower-level circulation patterns of the high-altitude trough, shear line, and southwest jet stream, the urban cluster of the Guangdong-Hong Kong-Macao Greater Bay Area experienced light to moderate rainfall, deviating significantly from the forecasted heavy rain and local heavy rainstorm. This study explores the reasons for false alarms and predictability using ground observation data, radar data, ECMWF-ERA5 reanalysis field data, and ECMWF and CMA-TRAMS forecast data. The results indicate that the warm and moist airflow transported by the low-level jet stream was intercepted by the upstream MCS (mesoscale convective system) along the coastal area of western Guangdong, and inadequate conditions of negative vorticity dynamics led to insufficient moisture, thermodynamic, and dynamic conditions over the urban cluster, preventing the triggering of heavy precipitation. In addition, the 700 hPa westerly flow guiding the airflow and the stable low-level shear line, coupled with surface convergence lines, influenced the northward or southward movement of MCSs along the coastal and inland regions of western Guangdong. The weak and discontinuous intensity of echoes in the upstream Zhaoqing region further hindered the influence of surrounding echoes on the urban cluster. Numerical forecast models ECMWF and CMA-TRAMS overestimated the 850 hPa windspeed and 925 hPa meridional windspeed, resulting in the forecasted urban cluster experiencing heavy rain. Sensitivity tests of wind fields indicate that the 850 hPa wind field information is more sensitive to precipitation in the urban cluster. In this process, weak signal correction can be achieved in strong precipitation forecasts using the distinct signal of lower 850 hPa water vapor flux divergence compared to 925 hPa. Therefore, in the future, when the Guangdong-Hong Kong-Macao Greater Bay Area encounters similar warm-sector heavy rainfall events, adjustments to model forecasts can be made using specific 850 hPa elements such as wind speed, water vapor flux divergence, or specific humidity to enhance predictive accuracy.

1. Introduction

The mesoscale convective system (MCS) is a direct influencing factor for the occurrence of heavy rainfall, and its precipitation efficiency and duration are closely related [1–3]. When an MCS moves slowly or individual convective cells repeatedly pass through a fixed area, it is prone to trigger intermittent short-duration heavy rainfall. Conversely, if the MCS moves quickly, has a short impact duration, or is of weaker intensity, it only brings about light precipitation [4–6]. In the multiscale systems that influence heavy rainfall in southern China, the low-level jet stream is an important weather system for heavy rainfall formation [1, 7–11]. On one hand, it acts as a moisture transport channel in the lower atmosphere, providing unstable warm and moist conditions. On the other hand, it acts as a dynamic force that enhances forced lifting through the convergence in the jet stream exit region. In China, there are two main types of low-level jet streams. One occurs between 1 and 4 km and includes the traditional 700 hPa and 850 hPa jet streams, also known as synoptic-scale low-level jet streams (SLLJ). The other occurs below 1 km and is known as the boundary layer jet stream (BLJ), influenced by the boundary layer, topography, and large-scale weather systems. In recent years, the roles of these two types of low-level jet streams in heavy rainfall events in southern China have attracted considerable attention [12–17].

Researchers such as Ding Zhiying et al. [18] have pointed out that warm-sector heavy rainfall in South China during May and June often occurs in the rear part of the 850 hPa low-level jet stream, within the area of southward wind convergence. Liang Shuang et al. [19] classified the low-level jet streams based on the synoptic patterns at 850 hPa into trough-type and cyclone-type jets. Despite differences in moisture transport and vertical wind shear, both types are significant components of extreme rainfall events in South China. Wunaigeng et al. [8] conducted statistical analyses using global gridded analysis data for the past decade, revealing that over 80% of warm-sector heavy rainfall events in the coastal belt of South China or the northern South China Sea are associated with the boundary layer low-level jet stream at 925 hPa. Research by Ye Langming et al. [20] on a specific South China rainfall process demonstrated that the 925 hPa low-level jet stream plays a crucial role as the main source of moisture, sustaining low-level energy. In addition, the occurrence of dual low-level jet streams is common in heavy rainfall events. Zhang et al. [9] pointed out that cases where both 800 hPa and 925 hPa low-level jet streams coexist account for 70% of warm-sector heavy rainfall events. DU et al. [10] analyzed a warm-sector coastal heavy rainfall event in South China, revealing that the development of warm-sector heavy rainfall is influenced by the convergence caused by the 925 hPa boundary layer jet stream and the joint effect of middle-level divergence caused by the synoptic-scale jet stream near 700 hPa.

LUO et al. [13] utilized 30 years of rainfall observation data from 1981 to 2012 to statistically identify three major heavy rainfall centers in South China with precipitation exceeding 1000 mm. These centers are located in the coastal areas of western Guangdong on the windward slope of the terrain, along the eastern coast of Guangdong, and in the central inland area around Fogang-Longmen. In recent years, research has been conducted from various aspects, including observation, statistics, case analysis, and numerical simulation, focusing on these three rainfall centers. While some regions within the densely populated, economically significant, and politically central Guangdong-Hong Kong-Macao Greater Bay Area do not meet the criteria for heavy rainfall centers, the occurrence of heavy rainfall in this area and the accuracy of rainfall forecasts are crucial for production, daily life, and decision-making.

However, there has not been much research on the precipitation mechanisms, mesoscale convective system characteristics, and variations in influencing systems specific to this region. Therefore, this study takes an instance of a false alarm heavy rainfall event that occurred in the Guangdong-Hong Kong-Macao Greater Bay Area from 12:00 on May 10th to 12:00 on May 11th, 2022 (UTC), as an example. Using ground observation data, radar data, ECMWF-ERA5 surface and upper-air reanalysis data, forecasts from the European Centre for Medium-Range Weather Forecasts (ECMWF) and China Meteorological Administration South China Sea Typhoon Numerical Forecast System (CMA-TRAMS), as well as the mesoscale CMA-GD model, the study analyses the characteristics of precipitation during this event, the development and causes of mesoscale convective systems, model errors, and the sensitivity of boundary layer wind fields. The aim of this study is to gain insight into the mechanisms behind such rainfall events in the Greater Bay Area and provide guidance for forecasting.

2. Data and Methods

2.1. Datasets

2.1.1. Observational Data. Observational data include South China Regional Automatic Weather Station Data. Wind Profiler Data from Hai Ling Island Station (Longitude 111.859°E, Latitude 21.572°N) and Xin Hui Station (Longitude 113.035°E, Latitude 22.532°N).

Dual-Polarization Radar Data from 15 radar stations across South China (Guangzhou, Shaoguan, Qingyuan, Zhaoqing, Meizhou, Heyuan, Shenzhen, Shanwei, Shantou, Yangjiang, Zhanjiang, Longyan, Xiamen, Haikou, Beihai). Single-Polarization Radar Data from 5 radar stations (Guilin, Liuzhou, Nanning, Wuzhou, Yongzhou). X-Band Dual-Polarization Phased Array Radar Data from Guangzhou. The locations of radar sites and wind profile sites are indicated in Figure 1.

2.1.2. Model Data. Model data include European Centre for Medium-Range Weather Forecasts (ECMWF) High-Resolution Numerical Weather Prediction Deterministic Forecast Products. Spatial resolution: 0.125°0.125° (surface) and 0.25°0.25° (upper air). Issued twice daily (00z, 12z).

The CMA-TRAMS South China Sea Typhoon Model Forecast Data are developed jointly by the China Meteorological Administration (CMA) and the Guangzhou Institute of Tropical and Marine Meteorology. It utilizes ECMWF data for initial conditions and has a spatial resolution of $0.09^\circ \times 0.09^\circ$. Forecasts are issued four times daily (00UTC, 06UTC, 12UTC, and 18UTC).

This study uses both models' 24-hour precipitation products from 12:00 on the 8th to 12:00 on the 9th, as well as 72-hour 3-hourly wind field products at 925 and 850 hPa and 12:00 on the 8th EC model forecast products for 925 and 850 hPa moisture flux divergence.

2.1.3. Reanalysis Data. The ERA5 dataset is the next-generation reanalysis dataset succeeding the European Centre for Medium-Range Weather Forecasts (ECMWF) reanalysis dataset. It has a spatial resolution of $0.125^\circ \times 0.125^\circ$. This study utilizes wind field data at pressure levels of 700, 850, 925, and 1000 hPa from 00:00 on May 10th to 12:00 on May 11th, 2022.

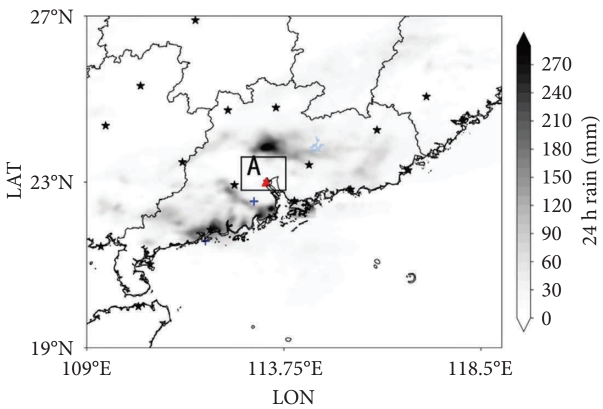

Figure 1: Distribution of accumulated precipitation (unit: mm) from 12:00 on May 10th to 12:00 on May 11th.

2.2. Model Scheme Design. In addition, the study applies the CMA-GD 3 km model, which is a nonhydrostatic model. It utilizes the WSM6 microphysics scheme, the MRF boundary layer physics scheme, the RRTMG-LW longwave radiation scheme, the RRTMG-SW shortwave radiation scheme, and disables cumulus convection parameterization. The model uses initial and boundary data from ECMWF's global resolution model with a resolution of $0.125^{\circ} \times 0.125^{\circ}$. The model starts with a longitude and latitude of 96°E and 16°N, respectively, has a horizontal grid of 913×513 grid points, 32 vertical layers, and a time step of 60 seconds.

3. Analysis of Precipitation Prediction Bias

3.1. Characteristics of Precipitation and Forecast Service Analysis. From 12:00 on May 10th to 12:00 on May 11th, 2022, the southern region of China experienced a weather event characterized by heavy to extremely heavy rainstorm, with localized severe weather (Figure 1). The distribution of precipitation was uneven, displaying distinct "rain nests" as features [13]. The areas with the strongest rainfall centers were located respectively along the western coast from Yangjiang to Jiangmen to Zhuhai to Zhongshan, along the eastern coast from Shenzhen to the southern parts of Huizhou, Shanwei, and Jieyang, and in the central mountainous region from Qingyuan to the southern parts of Shaoguan and the northern parts of Guangzhou, Fogang, and Longmen. The highest cumulative rainfall was recorded at the Sanshui National Meteorological Observatory in Zhongshan, with 408.5 mm. A total of 277 observation stations recorded over 100 mm of rainfall, 31 stations recorded over 250 mm, and in Yangdong District of Yangjiang City, the maximum hourly rainfall intensity reached 123.6 mm at 04:00 on the 11th.

Upon closer analysis, it is evident that the urban cluster of the Guangdong-Hong Kong-Macao Greater Bay Area, specifically the area extending from Foshan to the Guangzhou urban area to Dongguan (referred to as Region A, hereinafter referred to as the urban cluster), mainly experienced light to moderate levels of rainfall. Coupled with the suspension of classes mechanism, the occurrence of this severe rain event with false alarms in the urban cluster led to a certain social reaction.

Pentagram: South China Regional Radar Site; Cross: Wind Profile Site; Red Triangle: Panyu Phased Array Radar Site.

3.2. Objective and Subjective Forecast Situations. Comparing the 72-hour forecast with a 24-hour cumulative rainfall duration, initiated from 12:00 on the 8th, among multiple models (Figures 2(a)–2(c)), both the ECMWF and CMA-TRAMS models predicted heavy to extremely heavy rainfall in the urban cluster. Even when examining the 24-hour cumulative rainfall forecast for the subsequent 48 hours, starting from 12:00 on the 9th (Figures 2(b)–2(d)), although the coverage of extremely heavy rainfall reduced, the forecast still indicated heavy to extremely heavy rainfall, which was of a different magnitude compared to the actual observed precipitation in the region.

Considering the significant influence of synoptic-scale systems during this weather event and the fact that mainstream numerical forecast models consistently predicted widespread heavy rainfall, the subjective forecast conclusion was ultimately heavy to extremely heavy rainfall. In light of these factors, this stands as a clear case of forecast failure for the urban cluster.

4. Reasons for Forecast Failure Analysis

From the perspective of the large-scale circulation pattern, the 500 hPa geopotential height field at 12:00 UTC on May 10th (Figure 3(a)) shows a pattern with two ridges and one trough maintained in the mid-latitudes of Asia, which is one of the favorable circulation patterns for the premonsoon rainy season in South China. There are high-pressure ridges over the New Siberian Islands and the Okhotsk Sea, a low trough over the northern part of Northeast China, and a cutoff of the Northeast cold vortex. West of the cold vortex, there is a transition from the transverse trough to the vertical trough, while the southern side of the transverse trough at middle and low latitudes shows multiple shortwave trough activities. At 12:00 UTC on May 10th, the active southern branch trough of the Qinghai-Tibet Plateau was influencing the South China region from west to east. In addition, the transverse trough and the rear of the cold vortex guided cold air southward. By 00:00 UTC on May 11th, the 925 hPa wind field (Figure 3(b)) indicated that the cold air had reached the South China region and converged with the warm and moist southwest airflow ahead of the trough, resulting in stable low-level wind shear. At the same time, the Meng Bay storm gradually intensified, continuously transporting warm and moist southwest airflow to the South China region, with wind speeds reaching up to 12 m/s.

It can be observed that the favorable configuration of the high-altitude trough, shear line, and southwestern jet stream indeed provided favorable circulation conditions for heavy rainfall in South China. However, as is well known, the dynamic behavior of the middle-scale convective system, which is difficult to capture accurately in numerical models,

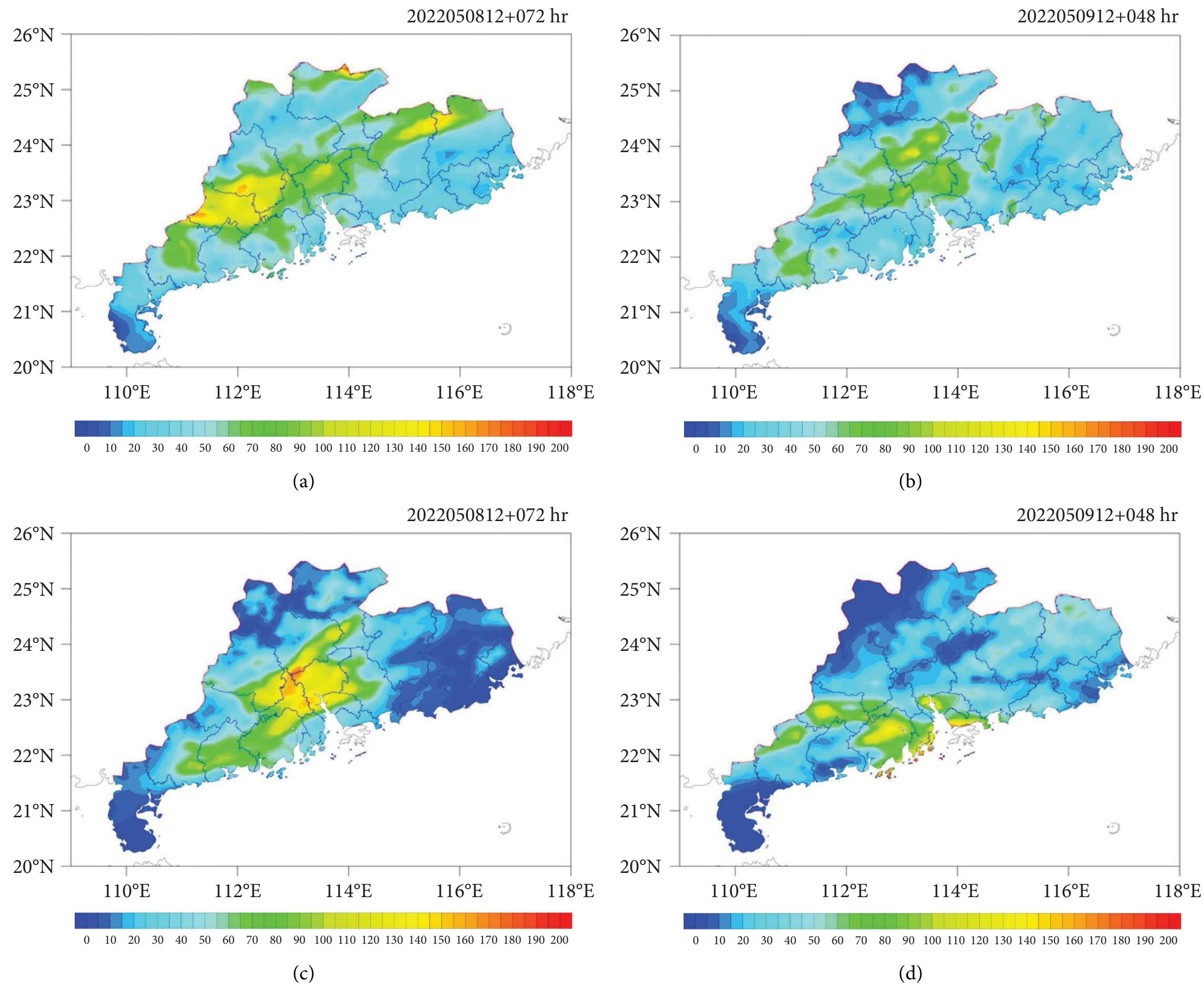

FIGURE 2: 24-hour accumulated precipitation forecast at 12:00 on May 11th: (a, b) ECMWF (c, d) CMA-TRAMS; initial conditions: (a, c) 12:00 on May 8th (b, d) 12:00 on May 9th.

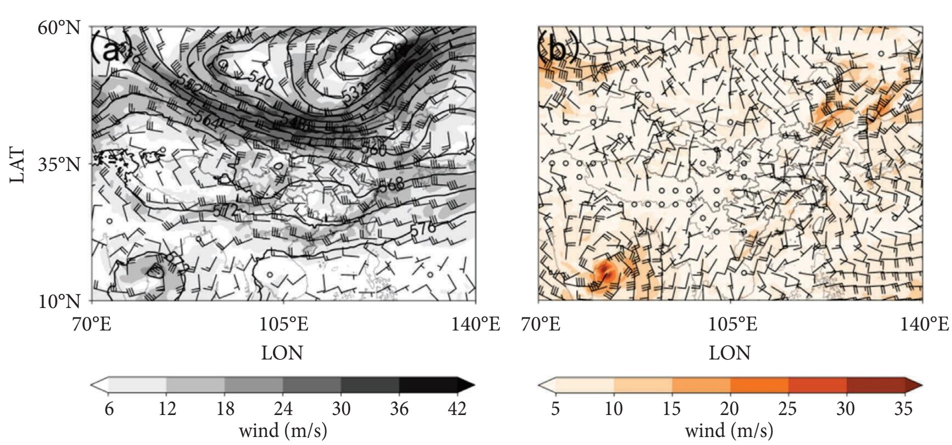

FIGURE 3: (a) 500 hPa geopotential height field at 12:00 on May 10th (contour, unit: dagpm) and wind field (shaded, unit: m/s); (b) 925 hPa wind field at 00:00 on May 11th (shaded, unit: m/s).

directly affects precipitation. Therefore, its structure and evolution influenced the significant discrepancies in precipitation observed in the urban cluster and the forecasted amount. Therefore, the subsequent analysis will delve into the occurrence and development of the middle-scale convective system on that day and its causes in detail, while also conducting a comprehensive analysis of the reasons for the forecast biases in mainstream numerical models.

4.1. Development and Analysis of the Mid-Scale Convective Systems. At 00:00 on the 11th, radar composite reflectivity indicated a "double rainband" precipitation pattern over the southern China region. This included MCS1 along the coastal area of western Guangdong and MCS2 from Fogang to Conghua inland, as shown in Figure 4. However, in the actual development process, neither of these MCSs had a significant impact on the urban cluster.

Examining the 925 hPa flow field at 00:00 on the 11th (as depicted in Figure 5), a favorable jet core is transporting moisture to the coastal area of western Guangdong, with wind speeds exceeding 14 m/s. This situation provides conducive conditions of moisture and warm, moist thermodynamic instability for the development of MCS1. In addition, analyzing near-surface wind fields using data from both inland and coastal wind profiling stations, it is evident that around 00:00 on the 11th, the near-surface wind speed at the coastal Hailing Island station reached around 12 m/s, while the inland Xinhui station had the maximum near-surface wind speed between 00:00 and 12:00, reaching 6 m/s. This indicates a significant weakening of near-surface moisture transport conditions over the inland areas, with moisture being intercepted by the upstream coastal regions. As a result, the thermodynamic conditions for triggering heavy precipitation from the near surface were weaker in the urban cluster compared to the coastal area of western Guangdong.

Analyzing the dynamic lifting conditions for the development of MCS1, this study selected the hourly variation of 500 hPa vorticity at the coastal Jiangmen station, the Tianhe station within the urban cluster, and the Conghua station in the northern region. It can be observed that around 22:00 on the 10th, the coastal region exhibited significant fluctuations in positive 500 hPa vorticity, reaching 5 × 10-5s-1, while the inland areas were consistently in a region of negative vorticity, signifying weaker dynamic lifting conditions than those along the coastal area (figure omitted). This is one of the main reasons why local convection within the urban cluster failed to trigger strong updrafts.

Regarding the movement of MCS1, even if it had affected the urban cluster during its development and movement, it still might have caused a certain level of heavy rainfall in the area. However, based on the radar composite reflectivity at 02:00 on the 11th (as depicted in Figure 6), MCS1 was mainly moving eastward along the coast, and there was not a significant northward movement of echoes. This is primarily due to the mid-level steering winds being dominated by westerly winds on the west side of the Pearl River Estuary. Although there was an increase in the southerly component over the urban cluster, resulting in a slight northward movement of MCS1 during its eastward movement, it was insufficient to affect the urban cluster significantly. Therefore, MCS1 did not cause significant heavy rainfall in the urban cluster.

MCS2 began developing gradually from 20:00 on the 10th and maintained its stability until around 14:00, without a noticeable southward shift by that time. As indicated in Figure 4 by the position of MCS2, analyzing the 925 hPa wind fields at 00:00 and 06:00 on the 11th, as well as the 10 m wind fields at 06:00 on the 11th (as depicted in Figure 7), it is apparent that the stable and weak dynamics of the low-level shear line and the mesoscale convergence line near the surface prevented significant southward movement of MCS2. Consequently, MCS2 did not exert a noticeable southward influence, which meant that it was unable to impact the urban cluster in terms of development and movement.

Around 11:00 before and after, a mesoscale convective system (MCS) developed gradually and moved eastward in the upstream region near Zhaoqing to the west of the urban cluster. Under its influence, the maximum composite reflectivity exceeded 50 dBZ, leading to short-duration intense precipitation of over 20 mm in Zhaoqing. By 12:00, the MCS moved closer to the urban cluster, causing a noticeable weakening of echo intensity. The maximum composite reflectivity dropped to around 35 dBZ, and between 13:00 and 14:00, the echo intensity further diminished (as shown in Figure 8).

Analyzing the mesoscale conditions contributing to this phenomenon (as depicted in Figure 9), due to the advance penetration of weak cold air, the surface convergence line had already affected the southern region of the urban cluster. In the urban cluster, dry and cold northward winds prevailed. This scenario weakened both the dynamic lifting convergence conditions necessary for convection development and the required thermodynamic conditions. Consequently, this affected the maintenance or development of intensity as the upstream MCS approached. Observing surface dew point temperatures, the area upstream near Zhaoqing maintained temperatures around 25°C, while in the vicinity of the urban cluster, temperatures were mostly between 23 and 24°C. This indicated that the atmospheric moisture conditions in the urban cluster were also less favorable compared to the upstream region.

Furthermore, using the X-band dual-polarization phased-array radar's reflectivity factor between 12:00 and 14:00 on the 11th to examine the minute-level intensity changes of the MCS echo (as shown in Figure 10), it can be observed that the MCS echo developed with relatively weak intensity and a lower vertical extent. The echo observations were mostly at radar elevation angles below 22°, and the maximum reflectivity factor ranged between 15 and 25 dBZ. Additionally, the echoes were discontinuous, particle sizes were small, and raindrop density was relatively low. Overall, the weak development intensity of the upstream MCS system affected the failure of the urban cluster to experience heavy precipitation.

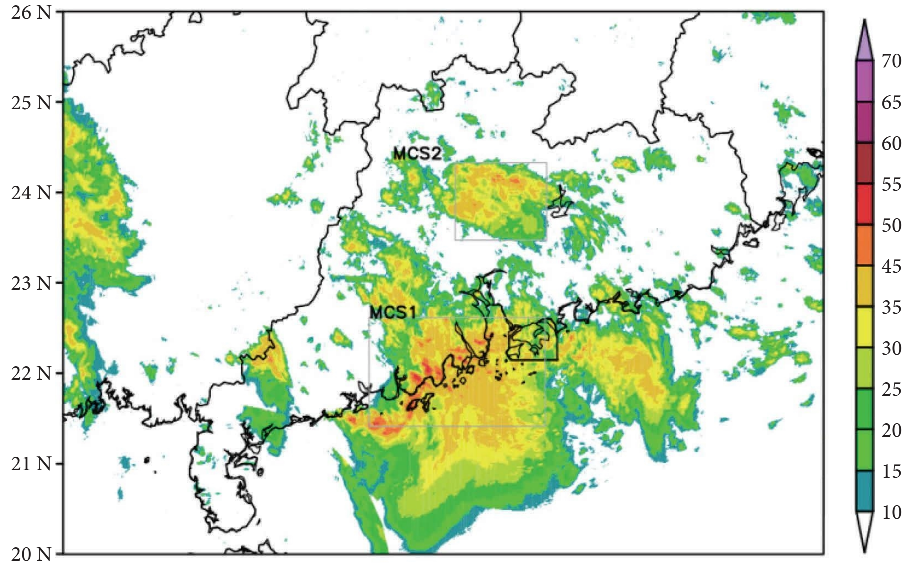

Figure 4: Radar composite reflectivity over South China at 00:00 on May 11th (unit: dBZ).

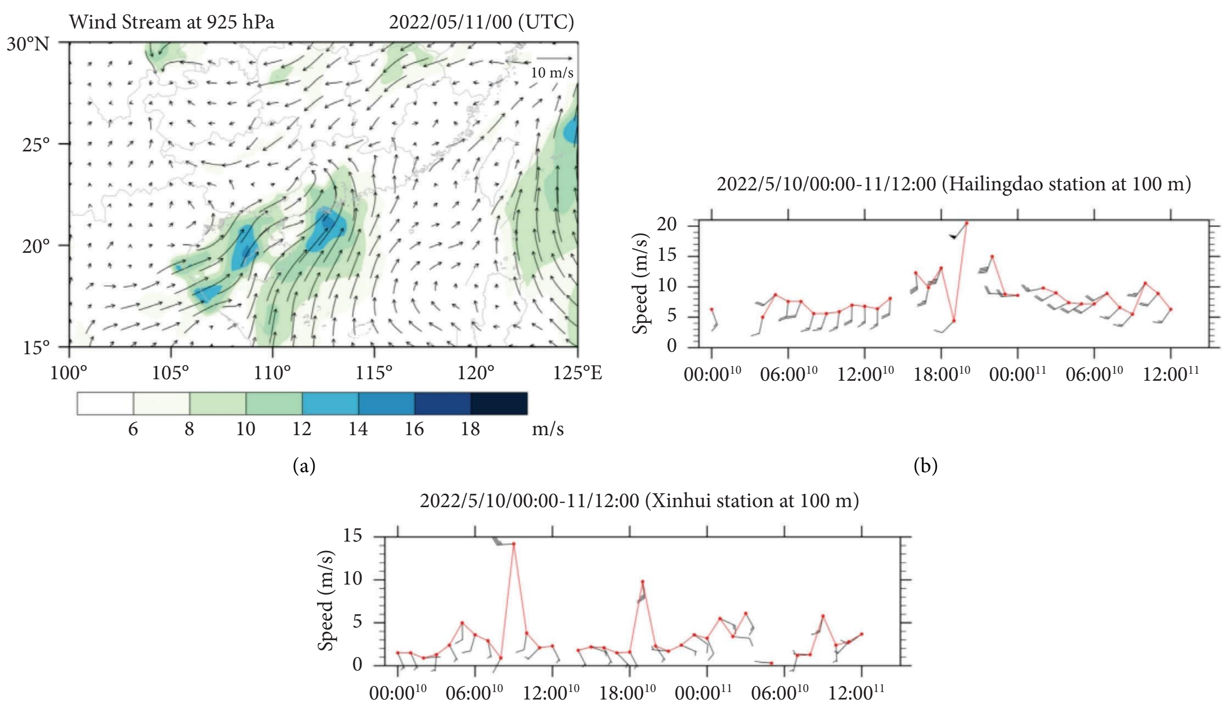

Figure 5: (a) 925 hPa wind field at 00:00 on May 11th (shaded, unit: m/s); wind fields at 500 m from 00:00 on May 10th to 00:00 on May 14th (unit: m/s); (b) Hailing Island Station; and (c) Xinhui Station.

Summarizing the analysis of the development and movement of mesoscale convective systems (MCS) upstream from the urban cluster, several factors come into play. The low-level jet core transports moisture to the coastal area of western Guangdong, but this moisture is intercepted, resulting in weaker near-surface and low-level wind fields downstream in the urban cluster. The insufficient moisture and thermodynamic conditions, combined with unfavorable 500 hPa vorticity conditions for convection development over the urban cluster, have collectively affected the occurrence of heavy precipitation.

Furthermore, the 700 hPa guiding airflow prevailing west of the Pearl River Estuary is primarily westerly, with a weak southerly component. As a result, the MCS over the coastal area of western Guangdong was unable to move northward to the urban cluster. For the MCS developing

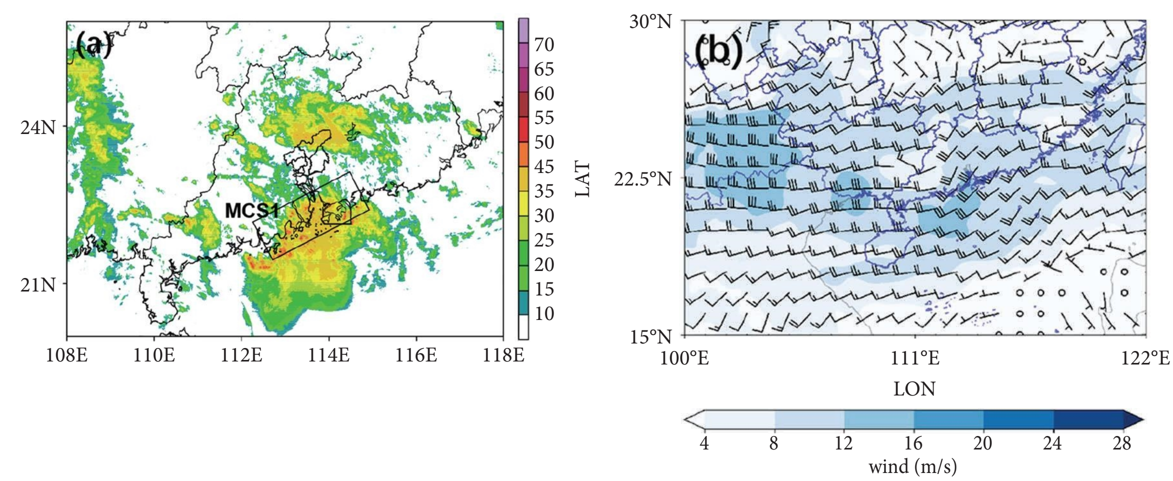

Figure 6: (a) Radar composite reflectivity over South China at 02:00 on May 11th (unit: dBZ); (b) 700 hPa wind field at 00:00 on May 11th (unit: m/s).

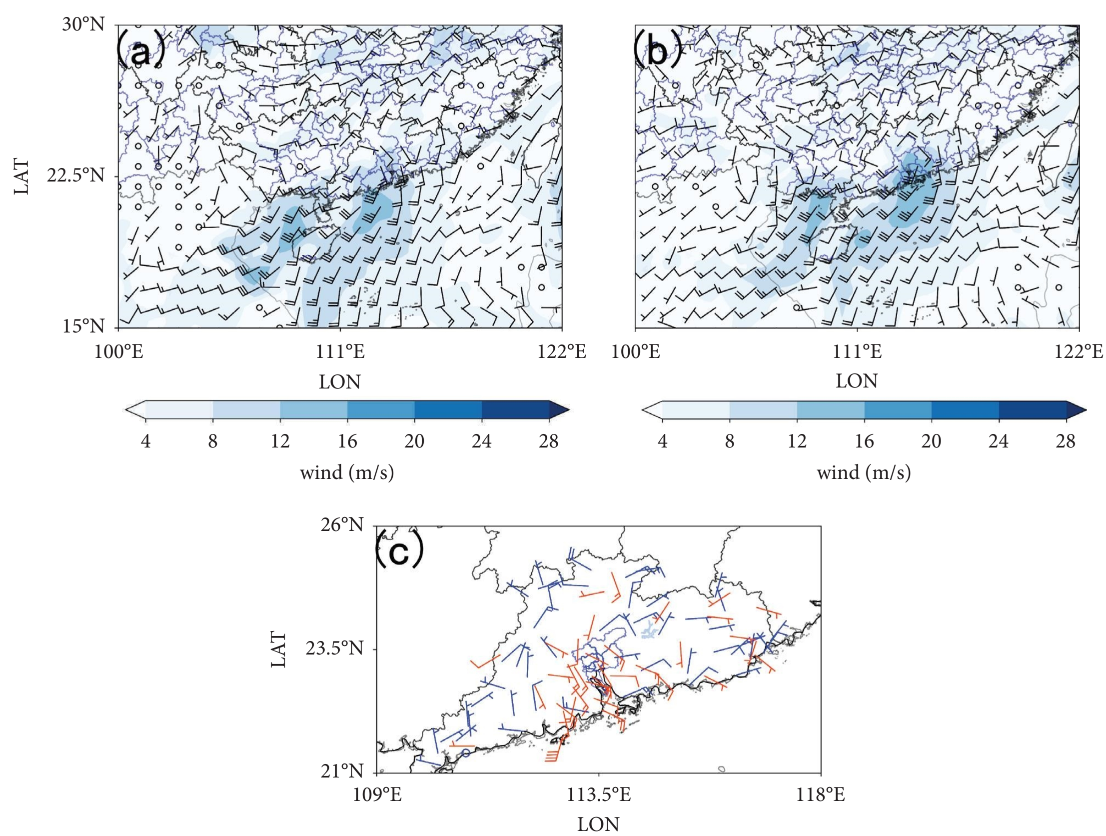

Figure 7: 925 hPa wind field (unit: m/s) at (a) 00:00 on May 11th; (b) 06:00 on May 11th; and (c) 06:00 on May 11th with 10 m wind from automatic stations (unit: m/s).

internally from Fogang to Conghua, the stable and weak dynamics of the low-level shear line and the mesoscale convergence line near the surface led to no significant southward movement, meaning this MCS did not impact the urban cluster either.

Regarding the echo development occurring around Zhaoqing by approximately 08:00 on the 11th, the echoes themselves only achieved a development intensity of 15–25 dBZ, and they were not continuous. Coupled with the shift to dry and cold northward winds over the urban cluster,

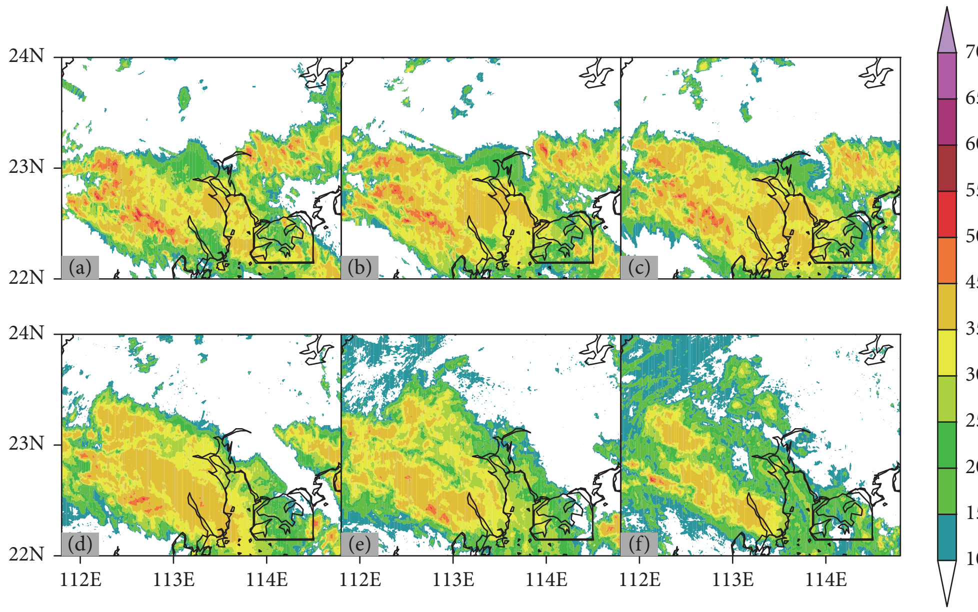

Figure 8: Radar composite reflectivity over the greater bay area (unit: dBZ) at (a) 11:00; (b) 11:36; (c) 12:00; (d) 13:00; (e) 14:00; and (f) 15:00.

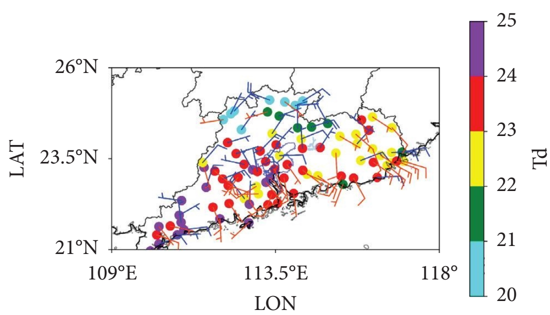

Figure 9: Wind field at ground automatic stations (vector field, blue: northerly wind, red: southerly wind, unit: m/s) and dew point temperature (data points, unit: °C) at 12:00 on May 11th.

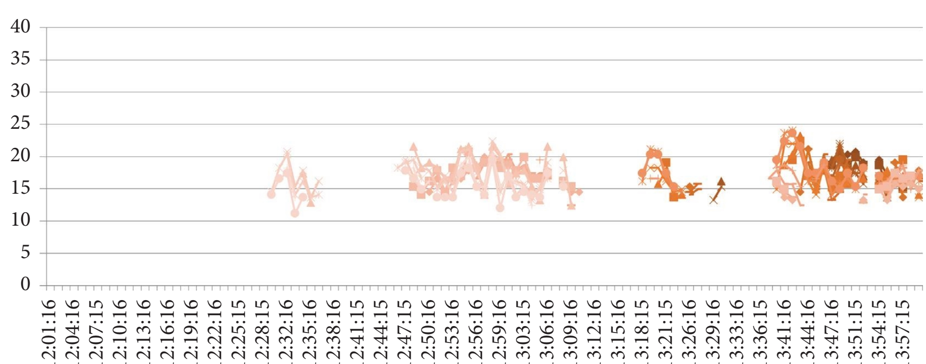

Figure 10: Intensity variation of X-band radar reflectivity factor from 12:00 to 14:00 on May 11th (unit: dBZ).

the thermodynamic conditions deteriorated. The surface convergence line was positioned southward, and moisture conditions were insufficient. These factors collectively led to a noticeable weakening of intensity as the upstream echoes moved towards the urban cluster, ultimately causing only light to moderate rainfall.

4.2. Model Forecast Bias Analysis. Numerical weather prediction models serve as the fundamental technological backbone for short-term forecasting. In the context of heavy rainfall forecasting in the warm region of South China, the positioning and characteristics of low-level jets and their upper-level cores are crucial focal points. In the case of the erroneous precipitation forecast for the urban cluster, what is the forecast performance of the numerical models concerning the mesoscale environmental wind fields? How does the sensitivity of the boundary layer wind fields impact the urban cluster's precipitation? The subsequent analysis delves into the deviations within the model wind fields and their sensitivity, aiming to provide a basis for assessing the predictability of such precipitation events.

Regarding the evaluation of the ECMWF and CMA-TRAMS models' performance in predicting the zonal and meridional winds at 850 hPa and 925 hPa over the South China region (range: 96.6°E to 122.76°E, 16.6°N to 30.76°N), certain biases have been identified (Figure 11). For the ECMWF model, it consistently overestimates the zonal winds at 850 hPa, with a maximum bias of up to 4 m/s across various forecast lead times. The bias remains persistent even in the latest forecast lead times. In contrast, the prediction of meridional winds at 925 hPa is generally underestimated by the ECMWF model. The initial forecast and the 54-hour forecast exhibit maximum biases of up to 4 m/s, though these biases tend to diminish with increasing forecast lead times.

For the meridional winds at 850 hPa and the zonal winds at 925 hPa, the ECMWF model tends to overestimate these winds, except for the 36-hour forecast of the meridional wind at 850 hPa, which is slightly underestimated by about 1.8 m/s. The maximum bias for these cases is around 2 m/s, smaller than the bias observed in the zonal winds at 850 hPa. Similar results are observed in the CMA-TRAMS model, with both models exhibiting a tendency to overestimate zonal winds at 850 hPa and to underestimate meridional winds at 925 hPa. However, the biases in the CMA-TRAMS model tend to be slightly smaller in certain forecast lead times, bringing them closer to the observed values. Considering the cumulative 24-hour precipitation, the overestimation of zonal winds at 850 hPa and zonal winds at 925 hPa in both ECMWF and CMA-TRAMS models may contribute to the prediction of heavy rainfall events in the urban cluster.

Based on the observed water vapor flux divergence fields at different time steps for 850 hPa and 925 hPa (Figure 12), it can be observed that at 00:00 on the 11th, both 850 hPa and 925 hPa formed a moisture convergence zone along the coastal area to the west of the Pearl River Estuary, with a maximum moisture flux divergence of 20 × 10-7 g·cm-2·hPa-1·s-1. This setup was conducive to significant heavy rainfall along the coast. Inland, particularly in the region from Foshan to Qingyuan, a more distinct moisture convergence zone was apparent at 925 hPa. However, the urban cluster exhibited a moisture flux divergence zone, which is not conducive to the occurrence of heavy rainfall. By 12:00 on the 11th, the moisture flux divergence zone over the urban cluster had not improved.

From the 48-hour forecast results of the ECMWF model, at 00:00 on May 11th (Figure 13), the 850 hPa moisture convergence zone did not form in the coastal area west of the pearl river estuary but was located further north, indicating a moisture convergence zone with a forecasted moisture flux divergence of 25 × 10-7 g·cm-2·hPa-1·s-1 from Zhaoqing to Yunfu City at 925 hPa. The urban cluster was forecasted as a clear moisture convergence zone at 925 hPa, which could easily mislead forecasters to predict significant rainfall in the urban cluster. By 12:00 on May 11th, weak moisture convergence was forecasted at 850 hPa over the urban cluster, and although the moisture flux convergence at 925 hPa had weakened in both range and intensity, it still indicated weak convergence conditions. Thus, from the temporal evolution of moisture flux divergence, the model consistently predicted warm and moist airflow transport to the urban cluster, forming convergence zones, which could create a misleading signal of heavy rainfall in the area.

Furthermore, the 24-hour forecast results of the ECMWF model did not show significant improvement in the moisture flux divergence at both 850 hPa and 925 hPa for 00:00 and 12:00 on May 11th, with the urban cluster still being forecasted as a clear moisture flux convergence area, which continued until 12:00 on May 11th (figure omitted). Thus, the model's prediction of a pronounced and sustained moisture flux convergence at 850 hPa and 925 hPa over the urban cluster can easily lead forecasters to misjudge it as a region of heavy rainfall.

5. Model Precipitation Simulation Analysis

Based on the above analysis, it can be observed that the models generally forecasted the large-scale circulation background correctly, predicting the occurrence of heavy rainfall events ranging from rain to heavy rainfall in the South China region. However, due to discrepancies in the forecasted environmental fields of the mesoscale convective systems, the development and evolution of the MCS in the urban cluster were overestimated, resulting in a false alarm. Further investigation is needed to determine which atmospheric layer, either in the lower levels (850 hPa and 925 hPa) or near-surface (1000 hPa), has a higher sensitivity to precipitation in the urban cluster.

In this study, sensitivity analysis was conducted using the mesoscale CMA-GD 3 km model for the false alarm precipitation event. This model is a non-hydrostatic model. The microphysics scheme used was the WSM6 scheme, the boundary layer physics scheme was the MRF scheme, the longwave radiation scheme was the RRTMG-LW scheme, and the shortwave radiation scheme was the RRTMG-SW scheme, with the cumulus convection parameterization scheme turned off. The model's initial and boundary conditions were provided by the ECMWF global analysis fields at a resolution of 0.125° × 0.125°. The model domain covered the area from 96°E to the west and 16°N to the north, with a horizontal grid size of 913 × 513 and 32 vertical levels. The time step was set to 60 seconds, and the integration period was from 00:00 on May 10th to 12:00 on May 11th, 2022. Three sensitivity experiments were designed (Table 1), where ERA5 reanalysis data replaced the initial and forecasted wind fields at 925 hPa, 850 hPa, and near-surface 1000 hPa for the respective time steps. The ERA5 reanalysis dataset has a temporal resolution of 1 hour and a horizontal resolution of 0.25° × 0.25°, serving as the next-generation reanalysis dataset after the ECMWF reanalysis dataset.

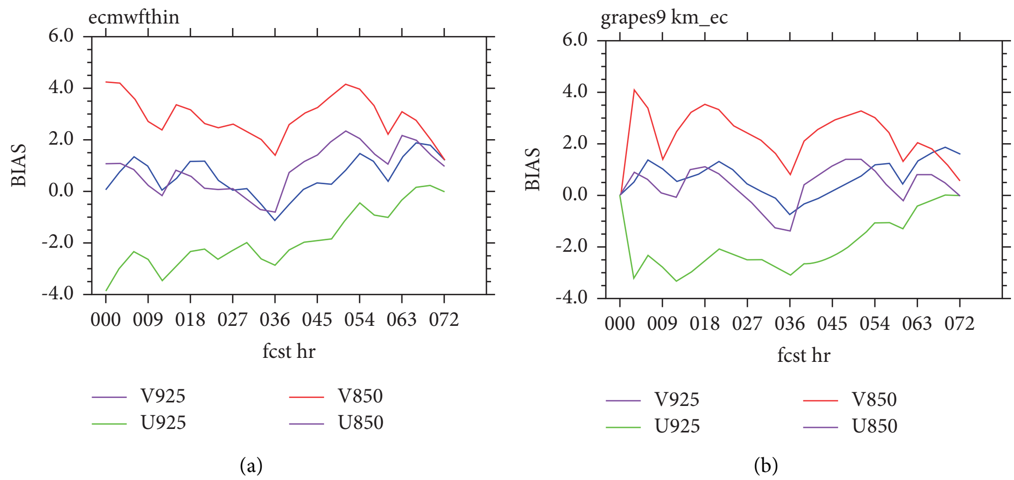

Figure 11: 72-hour BIAS of (a) ECMWF and (b) CMA-TRAMS models for the zonal and meridional wind speeds at 925 hPa and 850 hPa, respectively.

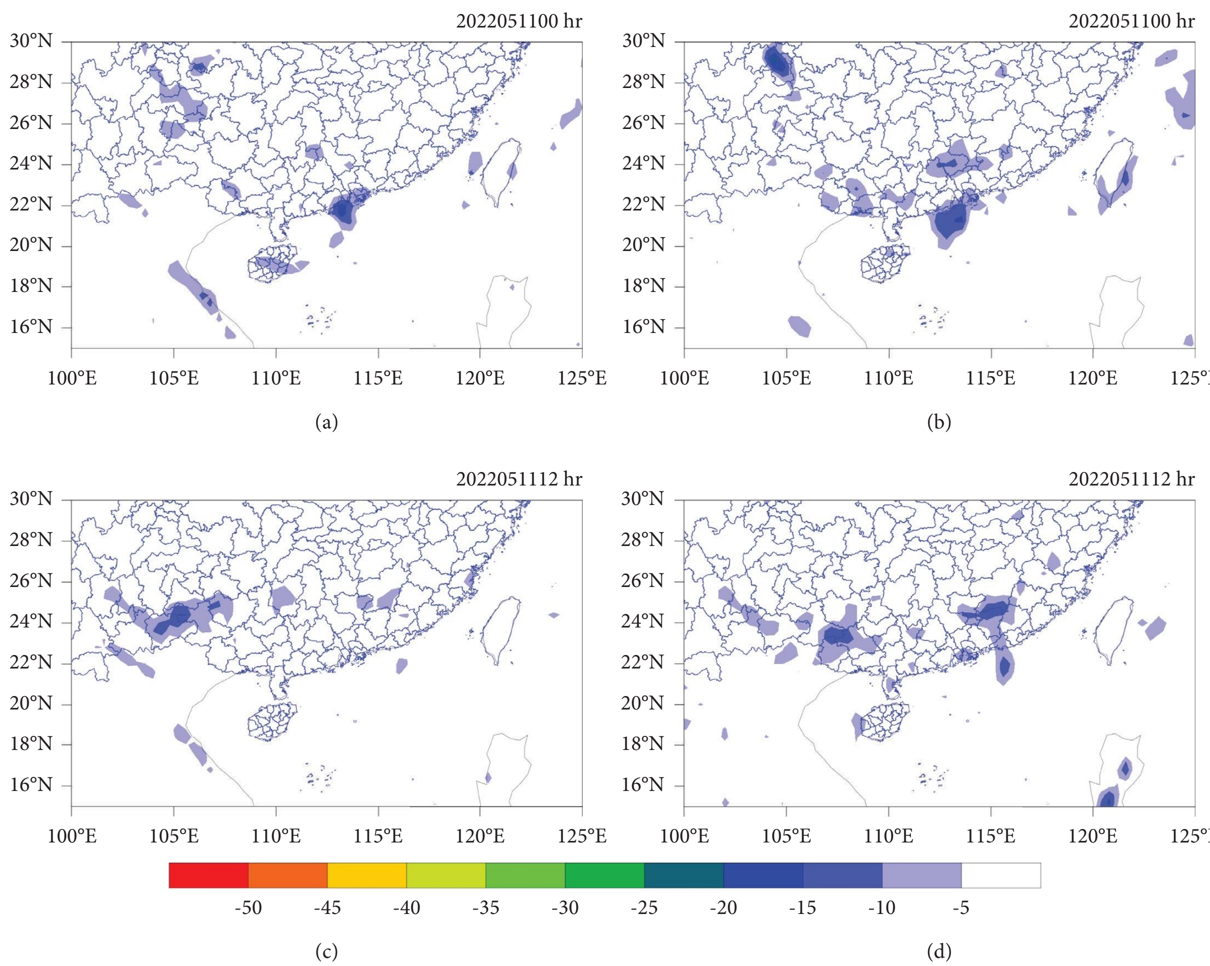

Figure 12: Observed water vapor flux convergence (unit: 10-7 g·cm-2·hPa-1·s-1) at 850 hPa (a, c) and 925 hPa (b, d) at 00:00 (a, b) and 12:00 (c, d) on May 11th.

From the comparison analysis of the observed and experimental results of 24-hour accumulated precipitation (Figure 14), the control experiment forecasted a significant precipitation belt over the central and northern parts of Guangdong, with the maximum accumulated rainfall reaching the level of heavy to severe rain and the area of

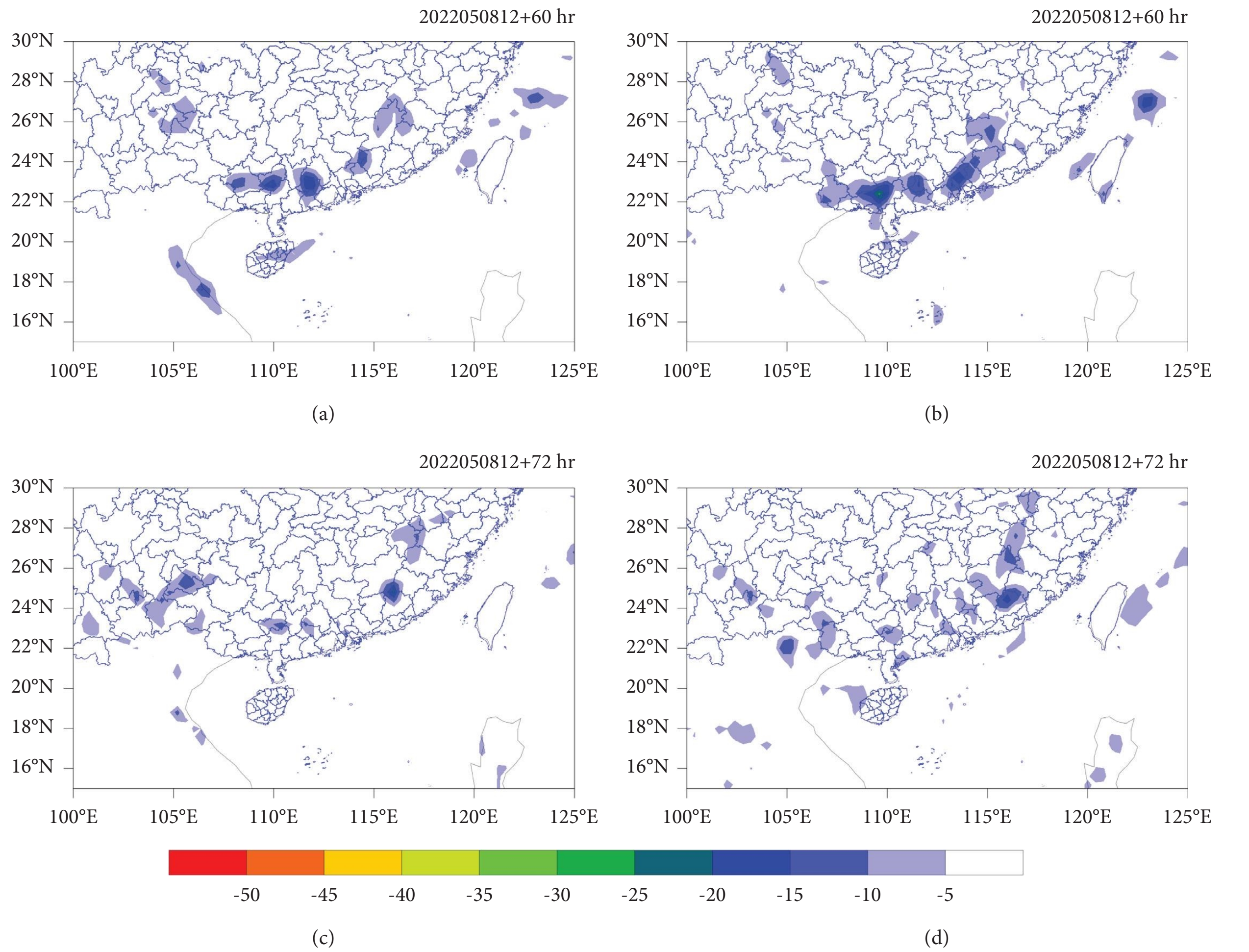

Figure 13: ECMWF model forecast of water vapor flux convergence (unit: 10-7 g·cm-2·hPa-1·s-1) at 850 hPa (a, c) and 925 hPa (b, d) at 00:00 (a, b) and 12:00 (c, d) on May 11th.

Table 1: Experimental table for wind field sensitivity analysis.

Control experiment (CTL)		ECMWF forecast analysis field
Sensitivity experiments	Replace 850 hPa wind field	Replace with ERA5 reanalysis data for 850 hPa wind field
	Replace 925 hPa wind field	Replace with ERA5 reanalysis data for 925 hPa wind field
	Replace 1000 hPa wind field	Replace with ERA5 reanalysis data for 1000 hPa wind field

heavy rain extended to the urban cluster. In the sensitivity experiment with revised 925 hPa wind fields, the area of heavy rain expanded further south but did not show significant improvement in weak precipitation over the urban cluster. Comparing the results of sensitivity experiments with revised 850 hPa and 1000 hPa wind fields, the area of heavy rain shifted northwards, and the urban cluster experienced mainly light to moderate precipitation, showing noticeable improvement compared to the control experiment and the sensitivity experiment with revised 925 hPa wind fields. In addition, after revising the 850 hPa wind fields, the model's precipitation forecast for the region from Fogang to Conghua to Qingyuan was closer to the observations, while revising the 1000 hPa wind fields resulted in a more significant improvement in the forecast of intense precipitation over the eastern coast of Guangdong compared to the other two levels. However, none of the revised wind fields showed considerable improvement for the heavy precipitation over the western coast of Guangdong, which is not the focus of this study and is not analyzed in detail here.

Based on the comprehensive analysis, the wind field at the lower level (850 hPa) is more crucial for the precipitation over the urban cluster, followed by the near-surface level (1000 hPa). Thus, the main reason for the overestimation of heavy to severe rainfall over the urban cluster by the ECMWF and CMA-TRAMS models is attributed to the overestimation of the 850 hPa wind fields and the misplacement of water vapor flux convergence.

In response to the analysis of key factors influencing model forecast biases and impact regions mentioned above,

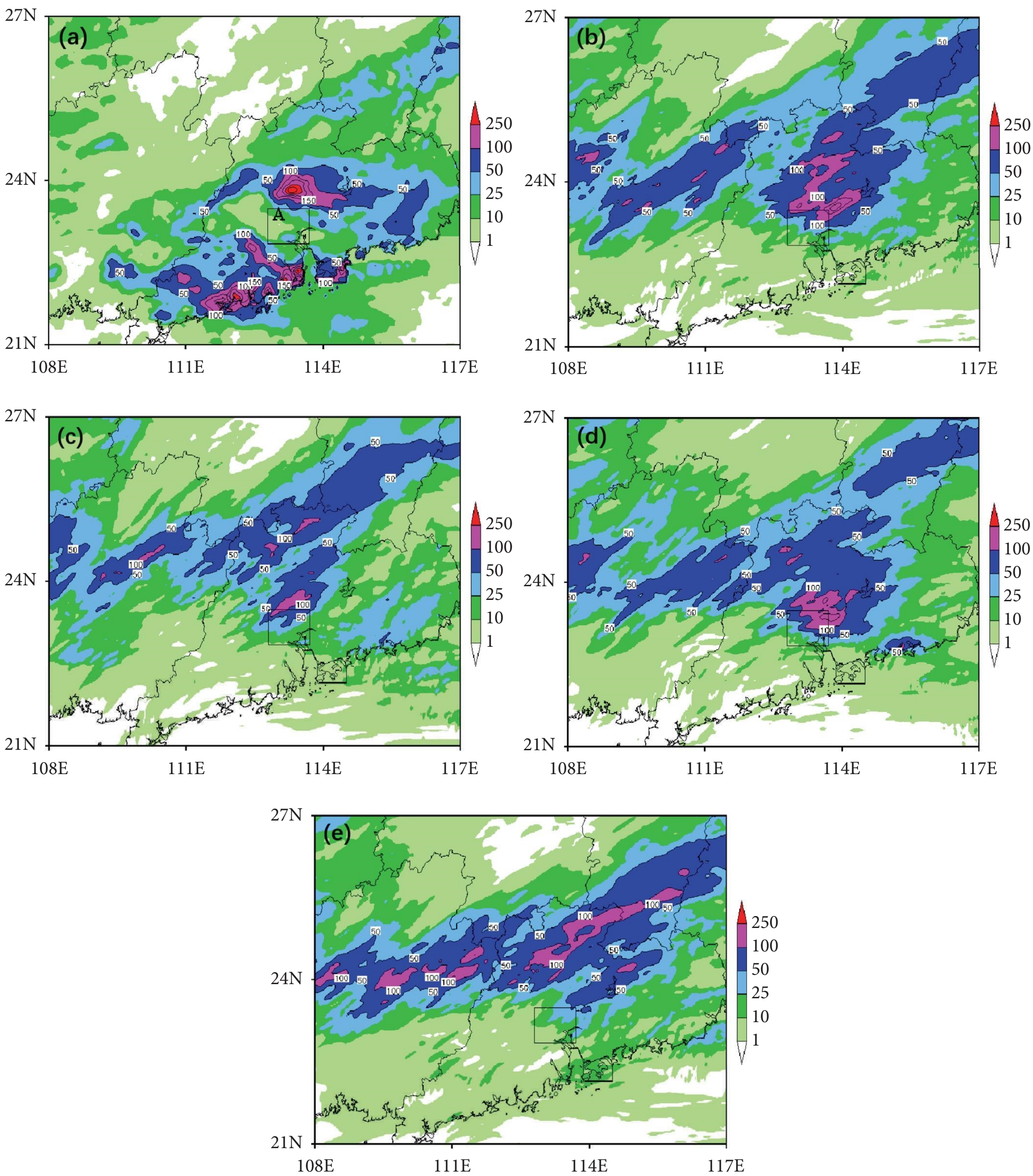

Figure 14: 24-hour accumulated precipitation from 12:00 on May 10th to 12:00 on May 11th: (a) observations, (b) control experiment, (c) 1000 hPa, (d) 925 hPa, and (e) 850 hPa.

how can we make corrections for weak signals in the forecast area based on other physical fields or key forecast factors when the model shows deviations in its predictions? In this case study, it was observed that the water vapor flux convergence at 850 hPa is significantly weaker than at 925 hPa. As the analysis indicated, the 850 hPa wind field is more sensitive to precipitation over the urban cluster. Therefore, a weaker water vapor flux convergence at 850 hPa can be considered as an indicator for reducing precipitation in the forecast.

Of course, in further research, one can statistically analyze the cases of strong precipitation occurrence and no strong precipitation occurrence over the urban cluster, considering parameters such as the water vapor flux convergence and specific humidity at 850 hPa. Based on threshold conditions, adjustments can be made to the forecast, providing another approach to revising model precipitation predictions. In addition, utilizing real-time vertical detection data from wind profilers, LIDAR wind profilers, and other instruments can help identify deviations in forecasted wind fields. Correcting short-term forecasts based on this comparison is also a topic worth exploring.

6. Discussion and Conclusions

In this study, we utilized ground observation data, radar data, ECMWF-ERA5 reanalysis data, and forecast products from ECMWF and CMA-TRAMS to analyze a case of false alarms in precipitation forecasts over the Guangdong-Hong Kong-Macao Greater Bay Area on May 10th, 2022, during a favorable atmospheric circulation configuration with an upper-level trough, shear line, and southwestern jet stream. The main conclusions are as follows:

(1) The primary reasons for the absence of heavy rainfall in the urban cluster during this event were as follows: First, the MCS (mesoscale convective system) off the coast of western Guangdong intercepted the warm and moist airflow transported by the low-level jet, resulting in insufficient moisture and thermal conditions over the urban cluster. In addition, unfavorable conditions with negative vorticity for convective initiation further hindered the occurrence of heavy precipitation. Second, the southwestern jet stream at 700 hPa, predominantly westerly, and the stable and inactive low-level convergence zones separately affected the MCS over western Guangdong and the MCS over the inland area from Foshan to Conghua, preventing them from reaching the urban cluster. Third, the intensity and continuity of echoes over the upstream area near Zhaoqing were weak, also contributing to the absence of heavy precipitation over the urban cluster.

(2) Both the ECMWF and CMA-TRAMS models exhibited evident biases. Overprediction of the eastward component of wind at 850 hPa and 925 hPa resulted in the false alarm of heavy rainfall in the urban cluster. Moreover, the persistent and significant water vapor flux convergence conditions led forecasters to judge it as a region of heavy rainfall.

(3) Analysis of wind field sensitivity experiments showed that information from the 850 hPa wind field was more sensitive to precipitation over the urban cluster. Signals of weaker water vapor flux convergence at 850 hPa than at 925 hPa during this event can be used to correct the forecast for regions with weak precipitation signals.

When applying short-term numerical forecasting models to analyze heavy rainfall events in warm regions, it is essential to not only focus on weather scale system changes and features but also pay attention to the occurrence and evolution of mesoscale convective systems and the sensitive atmospheric layers or weather systems in the region. The use of statistically derived, sensitive thresholds as conditions for precipitation predictability can help make appropriate adjustments to model forecasts.

Data Availability

Data sharing is not applicable to this article as no new data were created or analyzed in this study.

Conflicts of Interest

The authors declare that there are no conflicts of interest regarding the publication of this paper.

Acknowledgments

This study was jointly supported by the Key-Area R&D Program of Guangdong Province (2020B1111200001), China Meteorological Administration Review and Summary Special Project (FPZJ2023-091), Study on the Characteristics and Patterns of Ultra-Short-Term Precipitation and Evaluation of Short-Range Model Potential Forecast (M202303), Guangzhou Municipal Science and Technology Planning Project of China (202103000030), and Natural Science Foundation of Guangdong Province (2022A1515011814).

References

[1] L. He, T. Chen, and Q. Kong, "A review of studies on prefrontal torrential rain in South China," *Journal of Applied Meteorological Science*, vol. 27, no. 5, pp. 559–569, 2016.

[2] R. Zhang, Y. Ni, L. Liu, Y. Luo, and Y. Wang, "South China heavy rainfall experiments (SCHeREX)," *Journal of the Meteorological Society of Japan*, vol. 89, pp. 153–166, 2011.

[3] Y. Luo, R. Xia, and J. C. L. Chan, "Characteristics, physical mechanisms, and prediction of pre-summer rainfall over South China: research progress during 2008-2019," *Journal of the Meteorological Society of Japan*, vol. 98, no. 1, pp. 19–42, 2020.

[4] Z. Li, B. Liang, and C. Bao, "Mechanism and prediction of prerainy season heavy rainfall in South China," in *Collected Papers of Pre-rainy Season Heavy Rainfall in South China*, pp. 1–8, China Meteorological Press, Beijing, China, 1981.

[5] Q. Liang, S. Xiang, L. Lin, and W. G. Meng, "Mcs characteristics over SouthSouth China during the annually first rainy season and their organization types," *Journal of Tropical Meteorology*, vol. 28, no. 04, pp. 541–551, 2012.

[6] S. Huang, Z. Li, and C. Bao, *Rainstorms during Pre-rainy Season in South China*, Guangdong Science and Technology Press, Guangzhou, China, 1986.

[7] C. Bao, "Advances in heavy rainfall during the first rainy season in South China," *Acta Oceanologica Sinica*, vol. 8, no. 1, pp. 31–40, 1986.

[8] N. Wu, X. Ding, Z. Wen et al., "Contrasting frontal and warm-sector heavy rainfalls over South China during the earlysummer rainy season," *Atmospheric Research*, vol. 235, Article ID 104693, 2020.

[9] M. Zhang and Z. Meng, "Warm-sector heavy rainfall in southern China and its WRF simulation evaluation: a low-level-jet perspective," *Monthly Weather Review*, vol. 147, no. 12, pp. 4461–4480, 2019.

[10] Y. Du and G. Chen, "Heavy rainfall associated with double lowlevel jets over southern China. Part II: convection initiation," *Monthly Weather Review*, vol. 147, no. 2, pp. 543–565, 2019.

[11] G. Chen, W. Sha, and T. Iwasaki, "Diurnal variation of precipitation over southeastern China: spatial distribution and its seasonality," *Journal of Geophysical Research: Atmospheres*, vol. 114, no. D13, Article ID D13103, 2009.

[12] J. Min and N. Wu, "Advances in atmospheric predictability of heavy rain and severe convection," *Chinese Journal of Atmospheric Sciences (in Chinese)*, vol. 44, no. 5, pp. 1039–1056, 2020.

[13] Q. Wan, B. Wang, W. K. Wong et al., “The southern China monsoon rainfall experiment (SCMREX),” *Bulletin of the American Meteorological Society*, vol. 98, no. 5, pp. 999–1013, 2017.

[14] Y. Du and G. Chen, “Heavy rainfall associated with double low-level jets over Southern China. Part I: ensemble-based analysis,” *Monthly Weather Review*, vol. 146, no. 11, pp. 3827–3844, 2018.

[15] X. Chen, F. Zhang, and K. Zhao, “Influence of monsoonal wind speed and moisture content on intensity and diurnal variations of the Mei-Yu season coastal rainfall over South China,” *Journal of the Atmospheric Sciences*, vol. 74, no. 9, pp. 2835–2856, 2017.

[16] X. Chen, K. Zhao, and M. Xue, “Spatial and temporal characteristics of warm season convection over Pearl River Delta region, China, based on 3 years of operational radar data,” *Journal of Geophysical Research: Atmospheres*, vol. 119, no. 22, pp. 12447–12465, 2014.

[17] X. Chen, K. Zhao, M. Xue, B. Zhou, X. Huang, and W. Xu, “Radar-observed diurnal cycle and propagation of convection over the Pearl River delta during Mei-Yu season,” *Journal of Geophysical Research: Atmospheres*, vol. 120, no. 24, pp. 12557–12575, 2015.

[18] Z. Ding, C. Liu, and X.-Y. Shen, “Statistical analysis of the relationship among warm sector hevay rainfall, upper and lower tropospheric Jet Stream and south Asia high in May and June from 2005 to 2008,” *Journal of Tropical Meteorology*, vol. 27, no. 3, pp. 307–316, 2011.

[19] S. Liang, T. Xiao, and Y. Luo, “Relationship between extreme precipitation events and atmospheric rivers in the early flood season in SouthSouth China under the background of jet stream,” *Journal of Chengdu University of Information Technology*, vol. 35, no. 6, pp. 644–652, 2020.

[20] L. Ye and J. Miao, “Mesoscale analysis of a typical heavy rain event caused by returning flow in the warm sector in southern China,” *Torrential Rain and Disasters*, vol. 33, no. 4, pp. 342–350, 2014.